AIAA Propulsion and Energy Forum
July 9-11, 2018, Cincinnati, Ohio
2018 Joint Propulsion Conference

10.2514/6.2018-4818

Electric Solid Propellant Ablation in a Pulsed Electric Thruster

Matthew S. Glascock,[1]
Missouri University of Science and Technology, Rolla, Missouri, 65409, USA

Joshua L. Rovey[2]
University of Illinois Urbana-Champaign, Urbana, Illinois, 61801, USA

Electric solid propellants are advanced solid chemical rocket propellant that can be controlled (ignited, throttled and extinguished) with electric current. Work reported here focuses on application of electric solid propellant in a pulsed electric thruster similar to a pulsed plasma thruster. In the future it may be possible to develop a dual-mode electric solid propellant thruster that is switchable between steady applied electric current chemical mode and pulsed alternating electric current electric mode. Results presented here use a laboratory test thruster to create an arc discharge of 5-20 J per pulse in a cylindrical cavity of propellant. Results for Teflon and electric solid propellant are compared. Results indicate the electric solid propellant has higher ablation mass loss per pulse than Teflon (14.82 vs 7.17 μg/J), in agreement with theoretical analysis. The equivalent resistance and inductance of the arc plasma are 50 mΩ and 125 nH, respectively, for both propellants. Analyses indicate that the physical process of ablation is similar between propellants with thermal material properties driving the difference in the observed mass lost.

I. Nomenclature

V_0	=	initial capacitor voltage
C	=	capacitance of main capacitor
E_0	=	initial energy stored on the capacitor
$I(t)$	=	current measured through arc discharge
$L(t)$	=	time-variable inductance
$R(t)$	=	time-variable resistance
$V(t)$	=	voltage across the capacitor
L_0	=	inductance of circuit model at time zero
R_0	=	resistance of circuit model at time zero
$Q(t)$	=	time-variable charge stored on capacitor
Q_0	=	charge stored on capacitor at time zero
ω	=	frequency of undamped oscillatory current solution
P	=	oscillatory period of current solution
S	=	sum of squared residuals
r_i	=	residual value at time t_i
t_i	=	discrete values of time for measured current waveform
I_{EXP}	=	value of measured current at time t_i
I	=	value of LCR circuit model current at time t_i
$R_p(t)$	=	time-variable plasma resistance of arc discharge
E	=	actual energy dissipated in arc discharge
h_v	=	standard enthalpy (heat) of vaporization
h_f	=	enthalpy (heat) of phase change from solid to vapor
h_d	=	enthalpy (heat) of depolymerization

[1] Graduate Research Assistant, Aerospace Plasma Laboratory, Mechanical and Aerospace Engineering, 160 Toomey Hall, 400 W. 13th Street, Student Member AIAA.
[2] Associate Professor of Aerospace Engineering, 317 Talbot Lab, 104 S. Wright St., AIAA Associate Fellow.

h_a = activation enthalpy of exothermic reaction
C_p = standard specific heat at constant pressure
ΔH_f^0 = standard heat of formation at room temperature
η = fraction of E used for ablation of propellant

II. Introduction

Recent innovation in the solid rocket propellant field has led to the development of a new type of solid propellant that is safe, throttle-able, green propellant with at-will on-off capability. These electric solid propellants (ESP's) ignite and decompose when electric power is applied at sufficient current and voltage[1]. This decomposition is a highly exothermic process that generates hot gas at a burn rate that can be throttled by the applied current. Removal of the voltage and current extinguishes the reaction, at which point the reaction may be restarted digitally by reapplication of electric power. Because this reaction is only induced by electric current, ESP's are not susceptible to accidental ignition by spark, impact or open flame. These characteristics are extremely beneficial compared to traditional solid rocket propellants which are not throttle-able, toggle-able or insensitive to external ignition. The advent of ESPs expands the potential applications for solid propellant into areas previously infeasible.

ESP development began in the 1990's with the design of an automobile air bag inflator propellant (ABIP) using materials safe for unprotected human contact (i.e. "green" materials). This ABIP was ammonium nitrate-based and was later repurposed by the U.S. Air Force for use in other areas, including rocket propulsion. Shortly after, "ASPEN," the first digitally controlled extinguishable solid propellant was developed, which featured additives with the ammonium nitrate base to lower melting point and increase electrical conductivity[2]. This material showed performance metrics comparable to that of previous solid rocket propellants, but major problems existed with ignition. Further development led to an advanced formula with higher specific impulse and conductivity. The result was a high performance electric propellant, or HIPEP. In this solid energetic material, the ionic liquid oxidizer, hydroxyl-ammonium nitrate (HAN), exhibits a pyroelectric behavior unique to energetics. When electric power is applied, the proton transfer reaction between hydroxyl-ammonium and nitrate is promoted, and the level of nitric acid rapidly rises in the material eventually triggering ignition of the propellant. This behavior lends to use of the propellant in a dual-mode propulsion system wherein a high thrust chemical mode using direct current to incite pyroelectric gas generation is paired with a high efficiency electric mode. One promising electric mode configuration is a pulsed electric propulsion device known as the ablation fed pulsed plasma thruster. ABIP, ASPEN and HIPEP were tested in Aerojet's modular test unit (MTU) and reported impulse bits were all within 50% of the Teflon solid propellant that is typically used in such a device[1].

Pulsed plasma thrusters[3], or PPTs, have been in use since the first flight of an electric propulsion device in 1968. PPTs offer reliable impulse bits with higher exhaust velocities than possible using chemical thrusters, so long as electric power is already available on the spacecraft. Typically using the solid material polytetrafluoroethylene, commonly known as PTFE or Teflon, PPT's have the added benefit of inert propellant with no pressure vessel requirements. PPT's are typically used to fulfill secondary propulsion needs on spacecraft such as station-keeping[4-6] and attitude control[7,8]. Broadly, PPT's may be classified as possessing either rectangular or coaxial geometry[3]. Coaxial PPT's, like that of the University of Illinois PPT-3 and 4 begin with a central and a downstream electrode, often with a conical shape between[9,10]. The central or upstream electrode is typically cylindrical while the downstream electrode is ring-shaped, and either may be used as the positively charged electrode (anode). Solid propellant fills the space between electrodes and may be fed in through a breech. A capacitor or bank of capacitors is charged to a few kilovolts across the electrodes and an arc discharge is initiated by an ignitor. This ignitor is similar to an automotive spark plug but is usually smaller and custom-made in design and is always located in or near the cathode in a PPT. This arc discharge is fueled by ablation from the surface of the solid propellant, and consequently heats ablated propellant vapor to high temperature. The energy of this arc is sufficient to create large exit velocities for the propellant due to gas-dynamic acceleration, making the coaxial PPT a device dominated by electrothermal acceleration mechanisms. Ablation processes are at the core of PPT operation, and thus many studies on the ablation of PTFE exist in literature[11-17].

In this work, a pulsed electric thruster device was tested using both PTFE and the HAN-based HIPEP. For each propellant, the device was operated for 100 pulses in vacuum and the initial and final masses recorded to calculate the average ablated mass lost per pulse. Further analysis of the ablation process and an electrical circuit model provides comparison of the two propellants behavior. The objective of this work is to characterize the ablation process of the HIPEP material relative to the previously observed processes for PTFE.

III. Experimental

The following section provides details on the experimental apparatus used in this work. Details are given for the vacuum test facility where the work was conducted and the mass balance used for mass loss measurements. Discussion of the chemical makeup of the ESP used and propellant preparation procedures follows. Finally, the pulsed electric thruster test article and its associated electrical circuit are described.

A. Vacuum Facility and Mass Balance

The space and high altitude vacuum facility in the Aerospace Plasma Lab at Missouri S&T was used to conduct the tests in this work. The facility has a cylindrical test volume of about 6 ft (1.8 m) in diameter and 10 ft (3 m) in length. Four 89 cm diameter oil vapor diffusion pumps are the primary vacuum pumps and are backed by a Tokuda KP-7500BG rotary-vane and Edwards EH 4200 roots-blower pumps. The diffusion pumps are operated independently and with a single pump running (as was done during this work) the nominal base pressure is 2.5×10^{-5} Torr.

For mass loss measurements, a Sartorius QUINTIX125D-1S dual range semi-micro balance was used to measure the mass of propellant samples before and after testing. In the selected range, this balance has a capacity of 60 g and a readability of 0.01 mg. The factory reported repeatability of the balance is 0.02 mg. For measurements reported here the typical fluctuation in measurement was ±0.03 mg. The balance was used inside a nitrogen-purged glovebox such that the relative humidity was always less than 11% when mass measurements were obtained.

B. High Performance Electric Propellant

The ESP is a HAN-based solution solid manufactured by Digital Solid State Propulsion (DSSP) using benign processes and "green" ingredients, mixed in standard chemical glassware and cured at room temperature (35°C/95°F). It has a chemical composition of primarily HAN oxidizer (an inorganic ionic liquid) and polyvinyl alcohol (PVA) fuel binder, which make up 95% of the propellant. The ESP is initially a liquid and poured into a mold. It is then cured to form a soft solid with the appearance and texture of a soft pencil eraser. There are some key differences between the ESP and traditional Teflon (PTFE) PPT propellant. PTFE is a fluorocarbon solid, while the ESP is a soft solid mixture with composition given in Table I. In a typical PPT, the PTFE is an electrical insulator between the electrodes. The conductivity of the ESP in this work is comparable to "highly conductive" ionic liquids which have been selected as candidates for use in dye-sensitized solar cells[18]. With the ESP propellant the pulsed electric current could potentially be conducted through the ESP, initiating pyroelectric decomposition and creation of intermediates in the propellant. With PTFE an arc discharge is created near the surface of the solid PTFE, ablating the propellant via heat transfer. It is currently unclear how these propellant differences affect the operation and performance of a PPT using the ESP as a propellant.

Table I. Chemical composition of the High Performance Electric Propellant.

Chemical Name	Chemical Formula	Percentage by mass	Molecular Mass, g/mol
Hydroxyl Ammonium Nitrate (HAN)	$(NH_3OH)^+ NO_3^-$	75%	96
Polyvinyl Alcohol (PVA)	$CH_2CH(OH)$	20%	44
Ammonium Nitrate (AN)	NH_4NO_3	5%	80

C. Propellant Sample Preparation

The primary constituent of HIPEP is HAN, and HAN is known to by hygroscopic, and this behavior is reflected in the HIPEP formulation. For instance, in previous work[19] it was found that at standard laboratory atmospheric conditions, a ~1.2 g sample of HIPEP absorbed moisture from the atmosphere at a rate of 0.75 mg/min. Further, samples of HIPEP contain some percentage of water (DSSP estimates 1-5%) even when received from the manufacturer. In vacuum, this water will evaporate from the sample, skewing mass loss measurements unless special preparation procedures are implemented. In this work, HIPEP samples are only handled and measured while in a nitrogen purged inert environment glovebox with less than 11% relative humidity and pressure ~2 psig, and exposed to standard laboratory environment only briefly when being transferred to the test article in the vacuum facility.

A special drying procedure is used for fresh samples. First, the mass of a fresh sample is measured in the inert environment, where it is then loaded into a small sealable volume. This volume is then connected to a small vacuum facility and the system is kept at ~50 mTorr for at least 24 hours, allowing the moisture absorbed by the propellant to evaporate. This volume is then returned to the inert environment and vented allowing for measurement of the propellant "dry" mass. At this point, the propellant sample is loaded into the test article and undergoes arc discharge testing. After testing, a post-test "wet" sample mass is measured before reinserting the sample in the sealable volume and drying at 50 mTorr for another 24 hours. Finally, the post-test dry mass is measured. Basically the HIPEP is dried for 24 hours before arc discharge testing, and then another 24 hours after arc discharge testing, with mass measurements made directly after drying. This process was not conducted for the PTFE samples as testing showed that PTFE absorbed less than 0.1% mass of water over the course of many days of exposure to standard lab atmosphere. Quantitative details showing the evolution of HIPEP mass due to moisture content are presented in the results section.

D. Test Article

A coaxial geometry pulsed plasma discharge chamber was used for the ablation mass study. Figure 1 details the geometry of the discharge chamber. A circular stainless steel rod serves as the anode (positive) and a stainless steel plate with a circular hole serves as the cathode (ground). The assembly is housed in a nonconductive PEEK body. The propellant tube sample has length 12 mm and inner diameter 6.35 mm. Because HIPEP is conductive, the propellant is isolated electrically from the two electrodes by thin PTFE washers with inner diameter ~7 mm. The washers remain during PTFE testing to keep electrode spacing consistent between propellant samples.

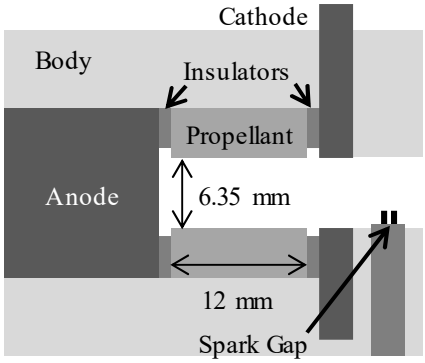

Figure 1: Diagram of the coaxial pulsed plasma discharge chamber test article.

The test article and the capacitor bank are inside the vacuum test facility. It is intended that the arc discharge occurs in the cylindrical cavity formed by the inner propellant tube wall and the anode end, with current flowing between the anode and cathode. Because the test article is at vacuum, the capacitor can be charged to a large voltage (1-5 kV) across the anode/cathode without initiating Paschen breakdown. Thus, the arc discharge breakdown is initiated by a small spark gap constructed of two tungsten wires cemented in a two-bore alumina tube with ~2 mm exposed tip lengths. The wire tips are located in the exhaust channel just downstream of the cathode as shown in Figure 1. A capacitor discharge ignition (CDI) circuit creates a small spark across the tungsten wire tips, introducing a number of electrons into the cylindrical cavity of propellant. These charge carriers allow the flow of current to begin between the electrodes, seeding the main arc discharge.

E. Electrical Setup

The electrical setup for the experiment is similar to that of a laboratory bench-top pulsed plasma thruster setup and is diagramed in Figure 2. A high voltage power supply is set to the desired discharge voltage, V_0, and is connected to ground. The power supply unit is a Glassman HV FJ05R24 model with a maximum DC voltage output of 5 kV and current output of 24 mA. This supply charges the main capacitor with capacitance C through a 500 Ω high power charging resistor, which also serves to prevent current from back flowing into the high voltage supply. The capacitance C is formed by a bank of eight 1 μF capacitors rated for 2.4 kV each. This bank was measured to have a capacitance of 8.055 μF. In this work, the bank was charged to voltages corresponding to stored energy levels of nominally E_0 = 5, 10, 15 and 20 J. During each discharge, an IPC CM-1-MG pulse current transformer measures the current, $I(t)$ through the anode side of the circuit. Not shown in the circuit diagram is the CDI spark gap circuit. The spark gap circuit is a single cylinder ignition coil with capacitance 0.47 μF and an output start voltage of 30-35 kV manufactured by CH Ignitions. The energy stored in the unit, about 40 mJ, is negligible relative to the main capacitor. This ignition unit is triggered manually by a push-button and isolated via an electromechanical relay.

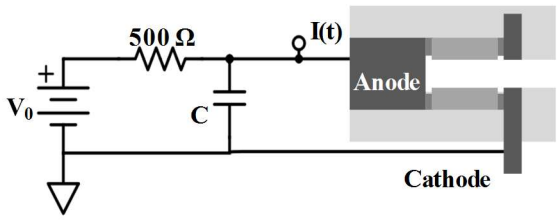

Figure 2: Circuit diagram for the pulsed plasma discharge chamber.

IV. LCR Circuit Model

Pulsed accelerators with thin arc current layers can be theoretically idealized as a switched inductance-capacitance-resistance (LCR) series circuit[20]. Consider the circuit diagramed in Figure 3. A capacitance *C* is initially charged to some voltage V_0, with stored initial energy E_0. At time zero, the capacitance is switched across a time-variable inductance *L(t)* and resistance *R(t)*. The initial inductance is determined both by circuit geometry and the inherent inductance of the capacitor. Initial resistance is a result of the external circuit resistance as well as a portion attributed to the arc discharge. Once the discharge is created, current *I(t)* flows through the circuit as the voltage, *V(t)*, dissipates from the capacitor.

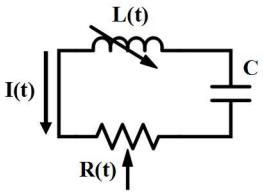

Figure 3: Ideal inductance-capacitance-resistance series circuit.

Examination of Maxwell's equation ($\boldsymbol{\nabla} \times \boldsymbol{E}$) around the circuit yields the differential Equation (1) for voltage and current in the single variable of time.

$$V(t) = I(t)R(t) + \frac{d}{dt}\big(L(t)I(t)\big) = IR + L\frac{dI}{dt} + I\frac{dL}{dt} \tag{1}$$

At time zero, the initial inductance L_0 and resistance R_0 are fixed values. Thus, a coaxial arc discharge can be thought of as a simple LCR circuit with fixed elements L_0, *C*, and R_0. If we consider now the time-varying charge stored on the capacitor, *Q(t)*, where $V(t) = Q(t)/C$, Equation (1) can be rewritten as a differential Equation (2) in terms of *Q(t)*; note that $I(t) = -dQ/dt$. The solution of Equation (2) has two forms for the initial conditions $Q_0 = V_0C$ and $I_0 = 0$, the overdamped form and the underdamped oscillatory form.

$$L_0\frac{d^2Q}{dt^2} + R_0\frac{dQ}{dt} + \frac{Q}{C} = 0 \tag{2}$$

For practical values of initial inductance, resistance and capacitance, the solution of the differential equation takes the underdamped oscillatory form. This solution in *Q(t)* can be rewritten in terms of the current *I(t)* as Equation (3) below.

$$I(t) = -\frac{dQ}{dt} = \frac{V_0}{\omega L_0}\, e^{-\frac{R_0 t}{2L_0}} \sin(\omega t)$$
$$\omega = \left(\frac{1}{L_0 C} - \frac{R_0^2}{4L_0}\right)^{1/2} \tag{3}$$

In this work, Equation (3) will be matched to the measured current waveform for a fixed V_0 test case. This is achieved by first matching the period of the sine function, $P = 2\pi/\omega$, to the numerically determined oscillatory period of the measured waveform from the test circuit. The period *P* is largely dominated by the value of L_0 such that it can be assumed R_0 is negligible in the period matching calculation and use $P = 2\pi(L_0C)^{1/2}$ to determine the value of L_0. The amplitude of the model prediction is determined largely by the value of R_0. With a fixed value of L_0, the resistance value can then be picked such that the model predicted values of *I(t)* best fit the measured current waveform for the first full period in a least squares sense. That is, R_0 will be iterated until *S*, the sum of residuals squared as defined in Equation (4) is minimized from time $t_0 = 0$ to $t_n = P$.

$$S = \sum_{all\ i} r_i^2 = \sum_{i=0}^{n} \left(I_{EXP}(t_i) - I(t_i)\right)^2 \quad (4)$$

In Equation (4), $I_{EXP}(t)$ is the experimentally measured current waveform, $I(t)$ is the current predicted by the LCR circuit model. The residual r_i is the difference between these values for all discrete values of time, t_i, that the current is measured by the oscilloscope. After the first full cycle (one-period), results show the measured current waveform has higher damping than the LCR model prediction (assuming constant R_0). Therefore we modify the LCR model to accommodate a linear increase in the resistance, with $R(t)$ starting at the end of the first period. The above process is then repeated with the variable resistance profile until S is minimized for the time $t_0 = P$ to $t_n = \infty$ where S is the sum of residuals squared as defined in Equation (4). This process is repeated for a representative discharge current waveform for each propellant and stored energy level.

V. Results

In this section, results from the experiment are presented along with brief discussion. First, the mass loss of HIPEP propellant samples during vacuum drying is reported. Ablation mass loss measurements of both propellants from the arc discharge test article follows. This section ends with presentation of the measured arc discharge current.

A. HIPEP Moisture Content

Using the propellant sample preparation procedures detailed in section III-C, the amount of water in a given HIPEP sample can be determined as a percentage of the sample mass. Details of mass measurements made of six samples of HIPEP are shown in Figure 4. These measurements were taken using the scale described in III-A and the error is $\pm 3\times10^{-5}$ g, or about 0.002% which is not visible on the scale of this figure. Figure 4a details the mass of three different HIPEP samples, beginning with the fresh sample mass when removed from original packaging at time 0 hours. Two measurements are made during the initial drying at 7 hours and 24 hours. The pre-test dry mass is recorded after 48 hours of drying, and then post-test wet mass recorded at 54 hours. Finally the post-test dry mass is recorded at 78 hours. These measurements illustrate the need for the propellant sample preparation procedures outlined in Section III-C. Propellant samples absorb water from the atmosphere, which evaporates in vacuum. The mass of the three samples decreases during pre-test drying at 5×10^{-2} Torr with measurements shown at 7, 24 and finally 48 hours. After 48 hours of vacuum drying the sample has reached a steady state in mass; this is the pre-test dry mass. Samples then undergo ablation testing in the test article described previously which typically lasts 6 hours. After testing, the facility is vented to atmospheric pressure during which time the sample is exposed to humid air and absorbs an unknown quantity of water. Samples then undergo the post-test drying process at 5×10^{-2} Torr and arrive at the post-test dry mass. Comparison of the pre- and post-test dry masses yields the mass lost due to the ablation of propellant in the test article.

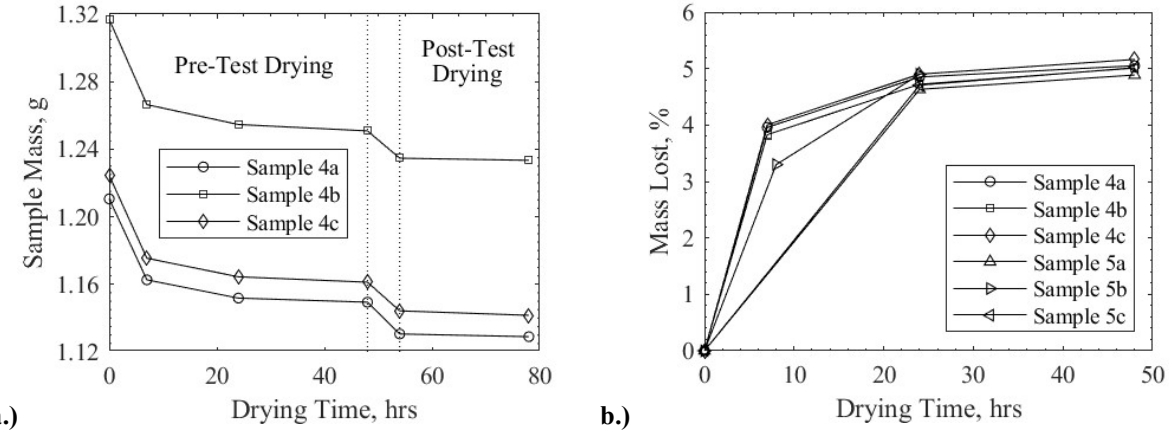

Figure 4: a.) Sample mass evolution for three HIPEP samples and b.) percent mass lost during drying of six HIPEP samples.

Figure 4b shows the mass lost during vacuum drying for six HIPEP samples as a percent of initial sample mass. The fresh samples of HIPEP have absorbed about 5% water by mass when removed from the original packaging received from the manufacturer. After 6-8 hours of vacuum drying, the sample mass has decreased by ~3-4%. After

24 hours of drying the samples have decreased by 4.5-5% in mass. Further mass lost after 48 hours of vacuum drying is minimal, and all six samples have decreased by an average of 5.0% in mass. Thus, the standard vacuum drying time for sample preparation was selected as 24 hours, at which point the measured mass of the sample is within 0.26% of the true mass (i.e., without water).

B. Ablation Mass Loss

Three samples of each propellant were tested and the mass loss measured at each discharge energy level. Energy levels of 5, 10, 15, and 20 J were investigated. Each propellant sample was prepared as described in section III-C. Prior to testing, the initial mass was recorded to an accuracy of ±0.03 mg. During testing, the charging voltage was kept constant for 100 pulses of the test article. The post-test mass was then recorded immediately after testing and re-pressurizing the vacuum facility. The mass loss is the difference in the pre- and post-test dry mass measurements. Table II details the mass loss values as well as calculated values for the change in mass loss-per-pulse and per-energy stored on the main capacitor (the specific ablation). Note that two samples of HIPEP were unable to be pulsed the desired 100 times during testing at the 15 J energy level due to a spark gap failure during testing. Those two tests were successfully repeated with 100 pulses and the results of both failed and successful test runs are presented here.

Table II: Ablation mass loss measurements for PTFE and HIPEP.

Propellant	Energy, J (Voltage)	Mass Loss, mg	Pulses	Δm/Pulse, μg	Δm/Energy, μg/J
PTFE	5.05 (1120 V)	3.68	100	36.8	7.29
		3.85	100	38.5	7.62
		3.79	100	37.9	7.50
	10.18 (1590 V)	8.20	100	82.0	8.06
		7.67	100	76.7	7.53
		6.97	100	69.7	6.85
	15.00 (1930 V)	9.48	100	94.8	6.32
		10.86	100	108.6	7.24
		10.54	100	105.4	7.03
	20.03 (2230 V)	13.38	100	133.8	6.68
		14.00	100	140.0	6.99
		13.85	100	138.5	6.91
HIPEP	5.05 (1120 V)	7.14	100	71.4	14.14
		8.55	100	85.5	16.93
		7.72	100	77.2	15.29
		16.11	100	161.1	31.90
	10.18 (1590 V)	20.42	100	204.2	20.06
		19.61	100	196.1	19.26
		17.42	100	174.2	17.11
	15.00 (1930 V)	22.79	100	227.9	15.19
		10.93	100	109.3	7.29
		16.60	100	166.0	11.07
		6.66	40	166.5	11.10
		8.97	75	119.6	7.97
	20.03 (2230 V)	17.64	100	176.4	8.81
		23.87	100	238.7	11.92
		28.52	100	285.2	14.24

The mass loss and pulse number are recorded during testing at each of the energy levels and reported in Table II. PTFE samples lost 37.7 μg per pulse for an initial capacitor voltage of 1120 V. Specific ablation is defined as the mass lost per Joule of energy stored on the capacitor. At 1120 V, the initial energy is 5.05 J and the specific ablation

of PTFE was 7.47 μg/J on average for the three test runs conducted. At 1590 V, or 10.18 J initial energy, PTFE ablated 76.1 μg on average per pulse with average specific ablation 7.48 μg/J. For 15.00 and 20.03 J initially stored on the capacitor bank, the average mass lost per pulse was 102.9 μg and 137.4 μg, respectively. For both of these energy levels the average specific ablation was 6.86 μg/J. In general, as the stored energy increases so too does the mass lost, but the specific ablation remains relatively constant with a ~8% decrease from 5 to 20 J.

For HIPEP, similar trends are observed. The average mass loss per pulse at 5.05 J initial energy was 98.8 μg, which yields a specific ablation of 19.56 μg/J. At initial energy of 10.18 J, HIPEP ablates 191.5 μg per pulse on average with average specific ablation 18.81 μg/J. When the capacitors were charged to 1930 V for an initial energy of 15.00 J, the average ablated mass was 157.9 μg per pulse for the five test runs at this energy level, including two which did not achieve the success criteria of 100 pulses. The specific ablation for this energy was 10.52 μg/J on average. Finally, for initial energy 20.03 J, the average ablation mass was 233.4 μg and average specific ablation 11.65 μg/J. For HIPEP, the estimated error in mass loss measurements is ±3.5 mg due to the 0.26% uncertainty in the initial mass measurement of each sample. Thus, for the HIPEP specific ablation calculations, the error is ±3.5 μg/J. Overall, the specific ablation remained roughly constant within the uncertainty from 5 to 20 J.

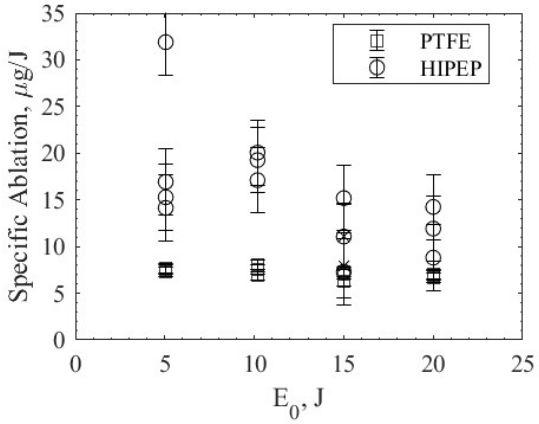

Figure 5: Specific ablation of PTFE and HIPEP materials for nominally 5, 10, 15 and 20 J stored energy.

The specific ablation for both propellants are shown in Figure 5 for the tested energy. The error bars are shown for both propellants: 3.5 μg/J for HIPEP and 0.5 μg/J for PTFE due to 0.26% and 0.025% uncertainties in initial sample mass measurements, respectively. Note that the two failed test runs of HIPEP samples at 15 J (only 40 and 75 pulses instead of the intended 100) are reported here and marked with an "x" symbol although they do not deviate significantly from other test runs at that energy. For the PTFE measurements, a specific ablation of 7.17 μg/J was measured on average over all pulses and energy levels. In contrast, the average over all pulses and energies for HIPEP was calculated to be 14.82 μg/J, a factor of 2.1 greater than the specific ablation of PTFE. More discussion on this observation is presented in section VI-B. Note that the average specific ablation decreases from 19.56 μg/J at the 5.05 J energy level to 18.81 μg/J at 10.18 J, but this is skewed by an anomalously high measurement of 31.9 μg/J at 5.05 J, the cause of which is unknown. This decreasing trend continues to the two higher energy levels, but this is likely an artifact due to the large error of the specific ablation measurements rather than a real phenomenon. Within the error, the trend is generally constant like that of PTFE. It is clearly seen that the variance in the specific ablation of HIPEP is much greater than that of PTFE. The standard deviation in specific ablation of HIPEP is 6.13 μg/J whereas the standard deviation is only 0.47 μg/J for specific ablation of PTFE.

C. Discharge Current

The discharge current is measured using a high current transformer. The variance in this current waveform is minimal from pulse to pulse at each selected voltage. Peak current typically varies less than 1% from pulse 1 to pulse 100 at 15 J, with the maximum variation over the current waveform less than 4%. Figure 6 shows a current measurement waveform for both PTFE and HIPEP at a stored energy level of 15 J representative of the discharge current for all pulses. The discharge current is very similar between propellants. Peak current in Figure 6a (PTFE) is 8.89 kA; by comparison, the peak current in Figure 6b (HIPEP) is 8.69 kA, a difference of only 2.3%. The first negative current peak has a difference of 6.3% between propellants and the second positive current peak is 19% different between the two propellants, with the current magnitude always greater for the PTFE discharge. The major difference between the two current waveforms is the lack of a third positive current maximum for the HIPEP discharge. This indicates that the circuit is more damped in the case of HIPEP.

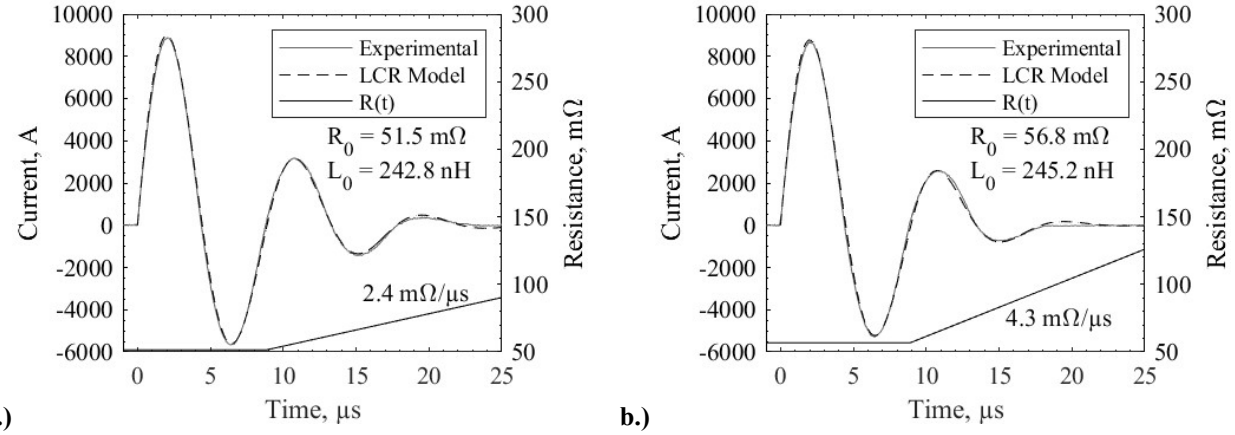

Figure 6: Discharge and LCR circuit model current for a.) PTFE and b.) HIPEP at the 15 J energy level.

The period of the waveform was also calculated by finding the first three roots of the experimental current data. A time-step of width 1×10^{-9} s was used on the oscilloscope recording the current transformer output for a precision of 0.001 μs for the calculated period. For the PTFE current in Figure 6a, the period was calculated to be 8.793 μs vs. the calculated period of 8.837 μs for HIPEP at the same energy. This difference of <0.5% indicates that the inductance of the circuit is nearly identical between propellants. These observations hold between propellants at each of the other energy levels. The peak current and period of the waveforms are tabulated in Table III. Overall the peak current for a HIPEP device is measured to be 0-2.5% less than the peak current for the PTFE device. The calculated period is less than 2% different over all energy levels.

Table III: Discharge current characteristics for PTFE and HIPEP.

Propellant	E0, J	Peak I(t), kA	P, μs
PTFE	5.05	4.98	8.970
	10.18	7.24	8.877
	15.00	8.89	8.793
	20.03	1.03	8.777
HIPEP	5.05	4.89	8.977
	10.18	7.07	8.980
	15.00	8.69	8.837
	20.03	1.03	8.743

VI. Analysis and Discussion

The following section presents details on theoretical analysis of the reported results and discussion on their significance. Details from the LCR circuit model current fit method are presented for both propellant configurations in the first subsection, followed by further investigation of the ablation energy for each propellant. A short subsection on the ablation process similarities between propellants is also included.

A. LCR Circuit Model

An LCR circuit model is used to generate a theoretical current waveform with the given C, V_0 and matched to the measured discharge current, as described in Section IV. The model is used to estimate a constant inductance value and resistance profile for the complete circuit. The resistance profile is a piecewise function made up of a constant initial resistance, R_0, followed by a linear increasing resistance that begins at the end of the first period of oscillation. The time at which the resistance is allowed to become linearly increasing is at the end of the first period, P, which was given in Table III for each energy level. Figure 6 shows the experimental data and the fitted LCR model current along with the calculated resistance and inductance for both PTFE and HIPEP at a stored energy level of 15 J.

The circuit model current best fits the experimental data in Figure 6 for both propellants with an initial inductance value of about 240 nH. For PTFE, the initial resistance value is calculated to be 51.5 mΩ while for HIPEP it is calculated to be 56.8 mΩ. After one period, the model current fits best with a slope of 2.4 mΩ/μs for PTFE and 4.3 mΩ/μs for HIPEP. The inductance is nearly identical between propellants as a result of the very similar period, which agreed to within 1%. As mentioned in Section V-C, the circuit appears to be more damped in the HIPEP case. These results agree, as the initial resistance is ~10% greater for HIPEP than for PTFE, and increases at a linear rate a factor of 1.8 greater for this energy level. Note that the calculated resistance and inductance of the circuit in the LCR model are equivalent values for the *entire* circuit. Both quantities represent contributions from three primary sources: the capacitor, the electrodes and the plasma[21]. At a frequency of 100 kHz, the dissipation factor of a single capacitor in the bank is rated less than 5×10^{-5} per the datasheet. Thus, the resistance of the capacitor bank at 100 kHz is on the order of 1 μΩ which is negligible here. At room temperatures, the resistivity of stainless steel is ~7×10^{-7} Ω-m and at 100 kHz the skin depth is 1.3 mm, which suggests the resistance of the anode and cathode electrodes is 1.2 mΩ and constant. Thus, the plasma resistance is the dominant resistance in the circuit, estimated to be 50-54 mΩ. From the manufacturer, the equivalent series inductance for one of the 1 μF capacitors in the bank is ~115 nH. The inductance of the test article is then ~125 nH and is independent of propellant used. The resistive power dissipated by the arc discharge can be computed using the integral of $P(t) = I_{EXP}(t)^2 R_p(t)$ where the plasma resistance is defined as $R_p(t) = R(t) - 1.2$ mΩ. For PTFE the calculated resistive power dissipation in the arc is $E = 13.71$ J, which is ~91.4% of the 15.00 J stored on the capacitor. For HIPEP, $E = 13.63$ J (90.9%) was dissipated by the arc discharge. The remainder of the stored energy on the capacitor was dissipated resistively through the other circuit elements (capacitor, electrodes, wires, etc.) and other loss effects not captured by this simple model. The above analysis was performed for each energy level and propellant, and the results are summarized in Table IV below.

Table IV: LCR circuit model analysis results.

Propellant	E0, J	L0, nH	R0, mΩ	R(t) slope, mΩ/μs	E, J	E/E0
PTFE	5.05	252.6	63.8	6.6	4.58	90.73%
	10.18	247.4	57.4	4.8	9.27	91.06%
	15.00	242.8	51.5	2.4	13.71	91.41%
	20.03	241.9	49.7	2.1	18.25	91.14%
HIPEP	5.05	252.9	70.5	9.9	4.55	90.14%
	10.18	253.1	59.8	6.0	9.22	90.55%
	15.00	245.2	56.8	4.3	13.63	90.89%
	20.03	240.1	51.3	3.6	18.13	90.49%

From these results, the equivalent circuit inductance is roughly constant between the propellants and with increasing energy, indicating that the conductivity of the HIPEP material is not contributing significantly to the inductance of the circuit. Even at low frequency, the calculated resistance of the conductive HIPEP sample is much greater than the equivalent circuit resistance implying the current is *not* being conducted through the propellant material itself. The initial plasma resistance for the HIPEP propellant is greater than for the PTFE propellant by about 7% on average, and the slope of increase after the first period is on average 1.5 times greater for HIPEP as well. Initial plasma resistance decreases with increasing energy for both propellants with correlation -1.03 mΩ/J for PTFE and -1.32 mΩ/J for HIPEP. Similarly, the slope of $R(t)$ also decreases with increasing energy. The actual arc energy calculated is only 92.5% of the stored energy on average versus 93.1% for PTFE. It is reasonable to assume that the temperature of the arc would increase with energy level and thus these results agree with Spitzer's relation for plasma resistivity, which decreases with increasing temperature[22]. Using Spitzer's relation for a plasma of cylindrical volume with diameter 6.35 mm, length 12 mm, uniform resistivity and resistance of 50 mΩ, the calculated temperature of the arc is ~3.8 eV. This arc temperature is typical of similar designs for a coaxial PPT using PTFE as propellant[3,23].

B. Ablation Energy Balance

Table II and Figure 5 detail the ablation mass loss and specific ablation values measured in this work. The specific ablation of PTFE is a constant value of 7.17 μg/J on average. Both the constant trend as well as the value of specific ablation are typical of a coaxial PPT[24]. Burton and Turchi reported similar values in the range of 1.5-10 μg/J for a number of PPTs, both coaxial and rectangular at varying energy levels[3]. The specific ablation of HIPEP is a factor of 2.1 greater than the specific ablation of PTFE, on average. In a previous investigation by the authors the specific

ablation for HIPEP was found to be 5.4 μg/J[25]. In this work, the specific ablation of HIPEP was measured to be 14.82 μg/J on average. Note that this work features a different experimental setup, both geometrically and electrically, compared to the previous investigation. These results indicate that the HIPEP material ablates more readily in an arc discharge than PTFE, with an average specific ablation a factor of 2.1 greater than PTFE.

For polymers, the heat of vaporization, h_v, is comprised of mainly the energy for phase transition to gas h_f and the energy for depolymerization h_d, with a smaller portion attributed to heating of the propellant from room temperature, $C_p\Delta T$. It is known that for PTFE the heat of vaporization to create pure C_2F_4 vapor is h_v = ~2×10^3 J/g[3]. At temperatures common in PPTs (i.e., >1 eV), PTFE vapor plasma is dominated by monatomic species and ions[26,27]. The energy required to dissociate C_2F_4 into monatomic species C and F is identical to the heat of formation, ΔH_f^0, which is 8.3×10^3 J/kg. Assuming that a fraction η of the total arc energy E (calculated in section A above) is deposited into the aforementioned devices, the theoretical ablated mass of PTFE, m_1, may be calculated by Equation (5).

$$m_1 = \frac{\eta E}{\left(h_f + h_d + C_P\Delta T\right) + \Delta H_f^0} = \frac{\eta E}{h_v + \Delta H_f^0} \tag{5}$$

HIPEP does not undergo a vaporization process like that of PTFE. The exact behavior of HIPEP at high temperatures is not currently known. However, it is known that the primary constituent of the material, HAN, undergoes a thermal decomposition process at a temperature of about 470 K. Lee and Litzinger[28] conducted a study of this process and found that the first reaction in the process produces hydroxylamine and nitric acid. Further, the rate of this reaction was estimated on the order of 10^{-10} sec, which is much faster than the 10^{-6} sec scale of the arc discharge current waveform. The activation energy h_a for this initiation reaction is 6.57×10^2 J/g. It is safe to assume that a HAN ($H_4N_2O_4$) vapor plasma at temperatures greater than 1 eV will be dominated by the presence of monatomic species and ions, as is the case for PTFE. The heat of formation of HAN is ΔH_f^0 = 3.78×10^3 J/g[29] and the specific heat at constant pressure of HAN, C_p = 2.29 J/g-K[30]. Following a similar approach to the ablation process of PTFE as described above, the arc energy can be assumed to be deposited into three primary processes. The first is propellant heating from room temperature to the decomposition temperature $C_P\Delta T$, then providing the activation energy h_a for the decomposition reaction, and finally dissociating the $H_4N_2O_4$ into monatomic species, which is equal to ΔH_f^0. Again it is possible to account for losses by assuming a fraction η of the total arc energy E is used in this process. The theoretical ablated mass of HIPEP, m_2, may be calculated using Equation (6).

$$m_2 = \frac{\eta E}{C_p\Delta T + h_a + \Delta H_f^0} \tag{6}$$

Examination of the ratio of the two theoretical ablation masses, assuming similar η, we find that m_2/m_1 = 2.14. This ratio is equivalent to the theoretical specific ablation (i.e., m_1/E_0) ratio because the stored energy is the same between propellants. Thus, the calculated specific ablation ratio of HIPEP to PTFE is 2.14 which is nearly identical to the measured ratio of 2.1 on average over the four energy levels. Further, comparing the measured average ablation mass of PTFE at the nominally 15 J level, m_1 = 102.9 μg/pulse, to Equation (5) we find that the above mentioned fraction is η = 7.7% of the total arc energy of 13.71 J. It is important to consider that the measured ablation mass also includes mass that evaporates from the hot propellant surface long after the high current discharge has ended, i.e. the late-time ablation mass. The late-time ablation of PTFE has been studied previously in literature, and is known to be in the range of 40% of the measured mass loss or more[31]. Per a previous investigation by the authors, the same is true for HIPEP, with an estimated late-time ablation fraction of ~45%[32]. If we assume then, that the plume is constituted by 60% of the measured ablation mass and has an average velocity of 10 km/s, the kinetic energy of the plume makes up ~22.5% of the energy dissipated in the arc. The largest portion of the arc energy is estimated to be transferred to the plume gas conductively. The heat transfer required to further heat the plume mass from the vaporization temperature of PTFE to 3.8 eV is calculated to be ~58.4% of the arc energy, taking the specific heat to be 3.0 kJ/kg-K. Together, the ablation, heating and acceleration of the plume mass is estimated to require 88.6% of the 13.71 J arc energy. The remaining 11.4% is likely radiated through the downstream orifice, transferred as heat conduction to the rest of the test article, and dissipated via other effects not accounted for here.

C. Ablation Processes

At high temperatures and over long (~ms) time-scales, it is known that HIPEP undergoes a thermal decomposition process while PTFE evaporates after depolymerization. However, the ablation processes studied in this work occur on much shorter time-scales, as the discharge current has a period of less than 10 μs. The above analyses show that the mechanism for ablation of HIPEP in a pulsed arc discharge is similar to that of PTFE. LCR circuit model analysis shows that the conductivity of the HIPEP material does not affect the discharge current significantly. Differences in

equivalent inductance are negligible and the difference in calculated plasma resistance is <10% between propellants. The specific ablation of HIPEP is roughly twice that of PTFE, but on the same order of magnitude. The difference in ablation mass between the two propellants can be directly attributed to differences in the material thermal and chemical properties. Further, previous work has shown that the fraction of late-time ablation mass is similar between propellants[19].

Many efforts to model the ablation of PTFE can be found in literature with context to PPT propellant as well as for high voltage circuit breakers. The analysis performed here suggests that these same models can be used to describe the ablation of the HIPEP material with consideration of the differences in material properties. Part of the inputs to these models, however, is a thermochemical model of the propellant vapor composition and transport properties as a function of the high temperatures expected in an arc discharge. Such models exist for PTFE using various methods[26,27], but none currently exist for HIPEP or even its primary constituent, HAN. Future HIPEP characterization work will need to be focused on developing this thermochemical model for high temperature vapor plasmas such that an ablation model similar to that used for PTFE may be constructed for the electric solid propellant HIPEP.

VII. Conclusions

Polytetrafluoroethylene (PTFE), or Teflon, and an electric solid propellant known as HIPEP were studied in a pulsed electric arc discharge chamber similar to a pulsed plasma thruster. The mass lost over 100 pulses of the arc discharge were recorded for samples of both propellants at nominal energy levels of 5, 10, 15 and 20 Joules. Discharge current was also measured and an LCR circuit model was fit to the measured current for constant inductance and initially constant resistance with a linear increase after one period.

Mass loss measurements indicate a specific ablation of 7.17 μg/J for PTFE and 14.82 μg/J for HIPEP. For both propellants, this value remains constant with increasing energy level, which is typical in coaxial PTFE PPT's. The factor of 2.1 greater specific ablation of HIPEP is attributed to key material property differences. Energy balance analysis was applied to both propellants where the arc energy is used to heat the propellant to the appropriate temperature, provide the energy to generate vapor at that temperature, then dissociate the molecule into monatomic species. This analysis suggests that ~7.7% of the arc energy is used to ablate propellant, and that HIPEP should have a specific ablation that is ~2.1 times greater mass than PTFE, agreeing with the experimental measurements.

The inductance-capacitance-resistance series model indicates that the constant inductance of the arc discharge is about 125 nH and does not change between propellants. The initial resistance is typically 50-60 mΩ for PTFE and between 3% and 10% greater for HIPEP, depending on stored energy. Because these values are very similar, the difference in conductivity of propellants does not significantly affect the electrical behavior of the arc discharge. Further, the arc temperature is comparable between propellants based on this result compared with known relation for plasma resistivity.

Results presented both in this work and in previous work comparing PTFE and HIPEP in pulsed electric devices suggest that the high temperature arc ablation process is very similar between propellants. The electrical characteristics of the arc plasma generated by each propellant vary by less than 10%. The ablation mass of PTFE is about 50% less than HIPEP for a given arc energy, and this is due to differences in propellant material properties. Further, the late-time ablation of both propellants is on the order of 50% of the measured propellant mass loss. While the long time-scale combustion characteristics of the propellants may be extremely different, the short-time scale ablation process is set apart merely by thermal material properties. Ablation models developed for PTFE may be confidently applied to at least HIPEP and potentially other electric solid propellants. Key inputs to these models will need to be examined and adjusted for material property differences, and quantify key chemical composition and thermal transport properties.

Acknowledgments

M. S. Glascock would like to graciously thank the NASA Space Technology Research Fellowship program, which has supported his Ph.D. research which includes this work through grant NNX15AP31H, with technical mentor Dr. Kurt Polzin. In addition to providing excellent input on theoretical considerations, Dr. Polzin has also graciously provided lab space and time during visits. The authors would also like to thank DSSP for providing custom made orders of the propellant samples, without which this work would not exist.

References

[1]Sawka, W. N., and McPherson, M., "Electrical Solid Propellants: A Safe, Micro to Macro Propulsion Technology," *49th AIAA/ASME/SAE/ASEE Joint Propulsion Conference*, AIAA, San Jose, CA, 2013. doi: 10.2514/6.2013-4168

[2]Sawka, W. N., U.S. Patent for a "Controllable Digital Solid State Cluster Thrusters for Rocket Propulsion and Gas Generation," No. 7958823 B2 and 8464640; June 14, 2011 and June 18, 2013.

[3]Burton, R. L., and Turchi, P. J., "Pulsed Plasma Thruster," *Journal of Propulsion and Power,* Vol. 14, No. 5, 1998, pp. 716-735. doi: 10.2514/2.5334

[4]Guman, W. J., and Nathanson, D. M., "Pulsed Plasma Microthruster Propulsion System for Synchronous Orbit Satellite," *Journal of Spacecraft and Rockets,* Vol. 7, No. 4, 1970, pp. 409-415. doi: 10.2514/3.29955

[5]LaRocca, A. V., "Pulsed Plasma Thruster System for Attitude and Station Control of Spacecraft," *First Western Space Congress*, 1970, pp. 688-702.

[6]Vondra, R. J., and Thomassen, K. I., "Flight Qualified Pulsed Electric Thruster for Satellite Control," *Journal of Spacecraft and Rockets,* Vol. 11, No. 9, 1974, pp. 613-617. doi: 10.2514/3.62141

[7]Gatsonis, N. A., Lu, Y., Blandino, J., Demetriou, M. A., and Paschalidis, N., "Micropulsed Plasma Thrusters for Attitude Control of a Low-Earth-Orbiting Cubesat," *Journal of Spacecraft and Rockets,* Vol. 53, No. 1, 2016, pp. 57-73. doi: 10.2514/1.A33345

[8]Rayburn, C. D., Campbell, M. E., and Mattick, A. T., "Pulsed Plasma Thruster System for Microsatellites," *Journal of Spacecraft and Rockets,* Vol. 42, No. 1, 2005, pp. 161-170. doi: 10.2514/1.15422

[9]Burton, R. L., Bushman, S. S., and Antonsen, E. L., "Arc Measurements and Performance Characteristics of a Coaxial Pulsed Plasma Thruster," *34th AIAA/ASME/SAE/ASEE Joint Propulsion Conference and Exhibit*, AIAA, Cleveland, OH, 1998. doi: 10.2514/6.1998-3660

[10]Wilson, M. J., Bushman, S. S., and Burton, R. L., "A Compact Thrust Stand for Pulsed Plasma Thrusters," *25th International Electric Propulsion Conference*, Cleveland, OH, 1997.

[11]Antonsen, E. L., Burton, R. L., Reed, G. A., and Spanjers, G. G., "Effects of Postpulse Surface Temperature on Micropulsed Plasma Thruster Operation," *Journal of Propulsion and Power,* Vol. 21, No. 5, 2005, pp. 877-883. doi: 10.2514/1.13032

[12]Gatsonis, N. A., Juric, D., Stechmann, D., and Byrne, L., "Numerical Analysis of Teflon Ablation in Pulsed Plasma Thrusters," *43rd AIAA/ASME/SAE/ASEE Joint Propulsion Conference & Exhibit*, AIAA, Cincinnati, OH, 2007. doi: 10.2514/6.2007-5227

[13]Keidar, M., Boyd, I. D., Antonsen, E. L., Gulczinski III, F. S., and Spanjers, G. G., "Propellant Charring in Pulsed Plasma Thrusters," *Journal of Propulsion and Power,* Vol. 20, No. 6, 2004, pp. 978-984. doi: 10.2514/1.2471

[14]Mikellides, P., and Turchi, P., "Modeling of Late-Time Ablation in Teflon Pulsed Plasma Thrusters," *32nd Joint Propulsion Conference and Exhibit*, AIAA, Lake Buena Vista, FL, 1996. doi: 10.2514/6.1996-2733

[15]Ruchti, C. B., and Niemeyer, L., "Ablation Controlled Arcs," *IEEE Transactions on Plasma Science,* Vol. PS-14, No. 4, 1986, pp. 423-434.

[16]Schönherr, T., Komurasaki, K., and Herdrich, G., "Propellant Utilization Efficiency in a Pulsed Plasma Thruster," *Journal of Propulsion and Power,* Vol. 29, No. 6, 2013, pp. 1478-1487. doi: 10.2514/1.B34789

[17]Seeger, M., Tepper, J., Christen, T., and Abrahamson, J., "Experimental Study on Ptfe Ablation in High Voltage Circuit-Breakers," *Journal of Physics D: Applied Physics,* Vol. 39, No. 23, 2006, pp. 5016-5024. doi: 10.1088/0022-3727/39/23/018

[18]Sigma-Aldrich, "Ionic Liquids for Electrochemical Applications," *Aldrich ChemFiles,* Vol. 5, No. 6, 2005.

[19]Glascock, M. S., and Rovey, J. L., "Ablation Mass Loss of an Electric Solid Propellant in a Pulsed Plasma Thruster," *35th International Electric Propulsion Conference*, ERPS, Atlanta, GA, 2017.

[20]Jahn, R. G., *Physics of Electric Propulsion*, New York: McGraw-Hill, 1968.

[21]Shaw, P., "Pulsed Plasma Thrusters for Small Satellites." Vol. Ph. D., University of Surrey, 2011.

[22]Spitzer, L., *Physics of Fully Ionized Gases*: Wiley, 1962.

[23]Bushman, S., and Burton, R. L., "Heating and Plasma Properties in a Coaxial Gasdynamic Pulsed Plasma Thruster," *Journal of Propulsion and Power,* Vol. 17, No. 5, 2001, pp. 959-966. doi: 10.2514/2.5849

[24]Rysanek, F., and Burton, R. L., "Effects of Geometry and Energy on a Coaxial Teflon Pulsed Plasma Thruster," *36th AIAA/ASME/SAE/ASEE Joint Propulsion Conference and Exhibit*, AIAA, Huntsville, AL, 2000.

[25]Glascock, M. S., Rovey, J. L., Williams, S., and Thrasher, J., "Plume Characterization of Electric Solid Propellant Pulsed Microthrusters," *Journal of Propulsion and Power,* Vol. 33, No. 4, 2017, pp. 870-880. doi: 10.2514/1.B36271

[26]Kovitya, P., "Thermodynamic and Transport Properties of Ablated Vapors of Ptfe, Alumina, Perspex, and Pvc," *IEEE Transactions on Plasma Science,* Vol. 12, No. 1, 1984, pp. 38-42.

[27]Wang, H., Wang, W., Yan, J. D., Qi, H., Geng, J., and Wu, Y., "Thermodynamic Properties and Transport Coefficients of a Two-Temperature Ptfe Vapor Plasma," *Journal of Physics D: Applied Physics,* Vol. 50, No. 39, 2017.

[28]Lee, H., and Litzinger, T. A., "Chemical Kinetic Study of Han Decompostion," *Combustion and Flame,* Vol. 135, No. 2, 2003, pp. 151-169.

[29]Ashcraft, R. W., Raman, S., and Green, W. H., "Ab Initio Aqueous Thermochemistry: Application to the Oxidation of Hydroxylamine in Nitric Acid Solution," *Journal of Physical Chemistry B,* Vol. 111, 2007, pp. 11968-11983.

[30]Decker, M. M., Klein, N., Freedman, E., Leveritt, C. S., and Wojciechowski, J. Q., "Han-Based Liquid Gun Propellants: Physical Properties," *US Army Technical Report BRL-TR-2864*, 1987.

[31]Spanjers, G. G., Lotspeich, J. S., McFall, K. A., and Spores, R. A., "Propellant Losses Because of Particulate Emission in a Pulsed Plasma Thruster," *Journal of Propulsion and Power,* Vol. 14, No. 4, 1998, pp. 554-559. doi: 10.2514/2.5313

[32]Glascock, M. S., Rovey, J. L., Williams, S., and Thrasher, J., "Observation of Late-Time Ablation in Electric Solid Propellant Pulsed Microthrusters," *52nd AIAA/SAE/ASEE Joint Propulsion Conference*, AIAA, Salt Lake City, UT, 2016. doi: https://doi.org/10.2514/6.2016-4845